Clay mineral diversity and abundance in sedimentary rocks of Gale crater, Mars

Thomas Bristow, Elizabeth Rampe, Cherie N Achilles, David F Blake, Steve J Chipera, Patricia Craig, Joy Crisp, David Des Marais, Robert T Downs, Ralf Gellert, et al.

Clay Mineral Diversity and Abundance in Sedimentary Rocks of Gale Crater, Mars

Authors

T. F. Bristow,[1*] E. B. Rampe,[2*] C. N. Achilles,[3] D. F. Blake,[1] S. J. Chipera,[4] P. Craig,[5] J. A. Crisp,[6] D. J. Des Marais,[1] R. T. Downs,[3] R. Gellert,[7] J. P. Grotzinger,[8] S. Gupta,[9] R. M. Hazen,[10] B. Horgan,[11] J. V. Hogancamp,[2] N. Mangold,[12] P. R. Mahaffy,[13] A. C. McAdam,[13] D. W. Ming,[2] J. M. Morookian,[6] R. V. Morris,[2] S. M. Morrison,[10] A. H. Treiman,[5] D. T. Vaniman,[14] A. R. Vasavada,[6] A. S. Yen[6]

Affiliations

[1]NASA Ames Research Center, Moffett Field, CA 94035, USA
[2]NASA Johnson Space Center, Houston, TX, 77058, USA
[3]Department of Geosciences, University of Arizona, Tucson, AZ, 85721, USA
[4]Chesapeake Energy, Oklahoma City, OK, 73154, USA
[5]Lunar and Planetary Institute, Houston, TX, 77058, USA
[6]Jet Propulsion Laboratory, California Institute of Technology, Pasadena, CA 91109, USA
[7]Department of Physics, University of Guelph, Guelph, Ontario N1G 2W1, Canada.
[8]Division of Geologic and Planetary Sciences, California Institute of Technology, Pasadena, CA, 91125, USA
[9] Department of Earth Science and Engineering, Imperial College London, London SW7 2AZ, UK.
[10]Geophysical Laboratory, Carnegie Institution of Washington, Washington, DC 20015, USA
[11]Earth, Atmospheric, and Planetary Sciences Department, Purdue University, West Lafayette, IN 47907, USA
[12]LPG, UMR6112, CNRS, Université Nantes, Université Angers, Nantes, France
[13]NASA Goddard Space Flight Center, Greenbelt, MD 20771, USA
[14]Planetary Science Institute, Tucson, AZ, 85719, USA

*Correspondence to: thomas.f.bristow@nasa.gov, elizabeth.b.rampe@nasa.gov

Abstract

Clay minerals provide indicators of the evolution of aqueous conditions and possible habitats for life on ancient Mars. Analyses by the Mars Science Laboratory rover, *Curiosity*, show that ~3.5 Ga fluvio-lacustrine mudstones in Gale crater contain up to ~28 wt.% clay minerals. Here we demonstrate that the species of clay minerals deduced from X-ray diffraction and evolved gas analysis show a strong palaeoenvironmental dependency. Whilst perennial lake mudstones are characterized by Fe-saponite, we find that stratigraphic intervals associated with episodic lake drying contain Al-rich, Fe^{3+}-bearing dioctahedral smectite, with minor (3 wt.%) quantities of ferripyrophyllite, interpreted as wind-blown detritus, found in candidate aeolian deposits. Our results suggest that dioctahedral smectite formed via near-surface chemical weathering driven by fluctuations in lake level and atmospheric infiltration, a process leading to

the redistribution of nutrients and potentially influencing the cycling of gases that help regulate climate.

Teaser

Clay minerals found in Gale crater, Mars, record surficial chemical weathering and changing conditions in an ancient lake.

Introduction

The Mars Science Laboratory (MSL) rover *Curiosity* has documented sedimentary rocks on the floor of Gale crater and lower slopes of the crater's central mound, Aeolis Mons (informally known as Mt. Sharp), since landing in August 2012 (*1,2)*. Early in the mission, at Yellowknife Bay (YKB) *(1)*, lacustrine mudstones of the Sheepbed member were shown to contain ~20 wt.% clay mineral, which was identified as Fe-rich saponite. Saponite was proposed as forming close to the time of sediment deposition by isochemical aqueous alteration of detrital olivine under anoxic to poorly oxidizing conditions *(3-5)*. By providing constraints on pH and possible substrates for chemolithoautotrophs during deposition, the clay minerals are key indicators of an ancient habitable lake *(1,3,4)*. D/H ratios of clay minerals combined with their mode of formation also constrain the global inventory of martian water ~3.5 Ga (*6*).

YKB gave an early glimpse of part of a spatially and temporally extensive Early Hesperian (~3.5 Ga) fluvial-lacustrine system that likely occupied much of Gale crater, which MSL continues to explore as part of its now >18 km traverse of the crater floor and lower slopes of Mt. Sharp *(2)*. Mineralogical and geochemical investigations of these sediments have revealed the dynamic natures of lake water chemistry and early diagenetic conditions, with evidence of redox stratification in the lake, and/or variations in pH and E_h during subsequent diagenesis *(7,8)*. Clay minerals were found in sandstones and mudstone samples stratigraphically above YKB at Windjana in the Kimberley formation, and various samples of the Murray formation outcrops in the Pahrump Hills (*7,9,10)* (Fig. 1, 2). The identified clay minerals largely belong to the 2:1 group (*7,9*), a family of phyllosilicates with a diverse range of physical, chemical, and crystallographic properties *(11-13)*. However, their low abundance (~10 wt.% or less), combined with XRD peak overlap from co-occurring pyroxene minerals *(7,9,10)*, prevent detailed crystallography and chemical characterization. As a result, key constraints on the origin and

genesis of clay minerals are not accessible. Here we provide these details for clay minerals in the four most recent drill samples of Murray formation mudstones, stratigraphically above the basal Pahrump Hills member (Fig. 1).

Results

The four Murray formation samples we investigated are drill powders, collected from a depth of 5 to 6 cm in the bedrock, by *Curiosity's* Sample Acquisition, Processing, and Handling (SA/SPaH). The samples in stratigraphic order, shown in Fig. 1, are: Oudam, from a ~25 m-thick unit of cross-stratified siltstones and very-fine grained sandstones of the Hartmann's Valley member, likely aeolian in origin, although a fluvial interpretation has been discussed; Marimba and Quela, which come from a ~30 m-thick package of finely laminated mudstones of the Karasburg member, representing a return to subaqueous deposition; and Sebina, from the Sutton Island member that consists of heterolithic mudstone-sandstones containing desiccation cracks and other sedimentary structures suggesting episodic drying and subaerial exposure of the Gale lake *(14-16)*. By examining the clay mineralogy of samples in their geological context, we constrain the timing, locus and mechanisms of clay mineral formation. Our findings are relevant to debates concerning surficial vs. crustal origins of clay minerals detected from orbit, which have implications for the planetary hydrology and climate of early Mars (*17-19*).

CheMin X-ray diffraction (XRD) analysis (Materials and Methods) show that clay minerals make up ~15 to 28 wt.% of the bulk rock with similar contributions to XRD patterns in Marimba, Quela and Sebina (Table 1). As observed in nearly every clay mineral bearing sample collected by MSL (Oudam is the exception, as described below), broad basal reflections at ~10° 2θ CoKα, (~10 Å), indicate the presence of 2:1 group clay minerals (Fig. 3A). The 02*l* clay mineral band, which is sensitive to the occupancy and species of cations within the octahedral sheets of clay minerals *(20)*, peaks at ~22.9° 2θ CoKα (4.50 Å; Fig. 3B). This band position is characteristic of dioctahedral 2:1 clay minerals *(13,20)*. Trioctahedral smectites in YKB samples (John Klein and Cumberland) have a distinctly different 02*l* band position (~22.7° 2θ, 4.58 Å) *(*Fig. 3B) *(3,4)*.

The CheMin sample cells maintain near-constant, very low humidity, which would promote loss of interlayer H_2O and collapse of smectite interlayers, making them difficult to distinguish from illite based on basal reflection position alone (*3*,*4*). However, illite, which

typically contains fixed K in the interlayer (*4,11-13*), does not appear to be a significant component of these samples based on the lack of correlation between clay content of Murray formation mudstones and K content of the bulk samples (Fig. S1). Smectitic clay minerals appear to be most abundant, with the K contents of samples accounted for by sanidine, jarosite and X-ray amorphous material (*10*, Table S1).

SAM evolved gas analyses (EGA, see Materials and Methods) give additional information on the nature of the octahedral sheets of the Murray clay minerals. The temperature of H_2O loss during heat-driven dehydroxylation of clay minerals is sensitive to cation content, occupancy, and the position of the vacant octahedral sites in dioctahedral clay minerals (*21-23*). Peak H_2O release of the Marimba sample occurred at 610°C and 780°C, indicating the presence of both dioctahedral and trioctahedral components, respectively (Fig. 4) (*21-24*). EGA data are inconsistent with the most Fe(III)-rich dioctahedral smectites such as nontronite, which have diagnostic dehydroxylation temperatures of <550°C (*21-24*). Comparison of the dioctahedral-assigned EGA peak at 610°C with laboratory studies of dehydroxylation temperature systematics as a function of Fe content suggest that the dioctahedral smectite likely contains ~5 wt.% Fe_2O_3, requiring at least half of octahedral sites be occupied by Al *(25).* The peak water release at 780°C, assigned to Mg-rich trioctahedral smectite, is higher than the 725°C peak observed for YKB samples (*24*), indicating that trioctahedral smectites in Marimba have a comparatively lower Fe content.

These observations are consistent with the CheMin XRD analyses. The intermediate position of the 02*l* clay mineral band is best modeled when measured clay mineral standards or structural models of both trioctahedral and Al-rich dioctahedral smectites are used in Rietveld refinements of the XRD patterns (Fig. 3C, Materials and Methods). Based on the combination of XRD, EGA, and bulk chemical data measured by the Alpha Particle X-ray Spectrometer (APXS) we find that a mixture of Al-rich dioctahedral and Mg-rich trioctahedral smectite is present in Marimba, Quela and Sebina. This is the first *in situ* detection of dioctahedral smectite in Gale crater.

There have been no direct orbital detections of phyllosilicate in strata traversed (so far) by Curiosity. Recent orbital VNIR spectra have documented signatures of Al/Fe-smectites in laterally (and presumably time equivalent) units of the Karasburg and Sutton Island members of the Murray formation (*26, 27,* Fig. S2). Our rover-based results presented here are the first

crystallographic ground truth of the thousands of orbital phyllosilicate detections, which are essential inputs for Mars science and mission planning (*17-19*). Our results confirm the presence of Al-rich dioctahedral smectite (albeit in conjunction with additional trioctahedral smectite) and other mineralogical information that helps constrain the origin and environmental implications of these clay minerals.

By incorporating structural models of clay minerals, with the *b*-unit cell parameter constrained by dehydroxylation temperatures observed in Marimba, Rietveld refinements of XRD patterns provide an estimate of the ratio of dioctahedral to trioctahedral smectites (Materials and Methods). The proportion of dioctahedral smectite increases up-section, with dioctahedral:trioctahedral ratios of 1:2, 1:1 and 5:3 for Marimba, Quela, and Sebina, respectively. The formation of Al-bearing dioctahedral smectites from basaltic precursors requires greater element mobility and more oxidizing conditions than the suboxic, isochemical aqueous alteration environments proposed for the Fe-saponite of YKB *(3,4)*. For example, in terrestrial weathering profiles of basaltic rocks, the initial alteration products of olivine typically contain trioctahedral smectite species with compositions (e.g., Mg/Fe) related to those of the primary minerals (*13*). As alteration progresses, trioctahedral smectites are replaced by dioctahedral clay minerals via removal of Fe^{2+} and Mg^{2+} and/or oxidation of Fe^{2+} and passive enrichment of Si and Al (*11-13*). Oxidizing conditions also tend to lower pH, which is less favorable for formation of Mg–trioctahedral clay minerals (*28*). As a consequence, trioctahedral smectites are rarely found in basaltic soils.

Formation of dioctahedral smectite formation is not restricted to surface weathering profiles; on a basaltic planet like Mars dioctahedral smectites could form in a variety of surface and subsurface aqueous environments (*17-19,28)*. Several observations indicate that the smectitic clay minerals in Marimba, Quela and Sebina were subject to modification or formed close to the time of deposition within the Gale sedimentary system. There is no evidence from orbital VNIR spectra for Al-bearing clay minerals in the rim and walls of Gale crater, suggesting that clay minerals we describe were not sourced there (*29*). The accompanying trends in sedimentary facies, as well as bulk mineralogy and geochemistry of mudstones, indicate that the occurrence of Al-bearing, dioctahedral smectite corresponds with a shift in environmental conditions and the degree of chemical alteration in Gale crater lake sediments. Fig. 2 shows the changes in abundances of environmentally sensitive mineral components along MSL's traverse, including: 1)

a transition from magnetite to hematite as the main Fe-oxide; 2) an increase in the abundances of Ca-sulfates, which appear to be matrix components above the Pahrump Hills member of the Murray formation and thus indicators of near-surface evaporative processes; and 3) an overall reduction in the quantity of reactive mafic minerals – pyroxene and olivine. These mineralogical trends broadly correspond with observed sedimentary indicators of shallowing and episodic lake desiccation (*14,16*). The observed increase in the degree of aqueous alteration of mafic detritus in the upper part of the Murray formation is also reflected in chemical indices of alteration derived from bulk geochemical analyses (*30*).

Our preferred mechanism for the production of Murray dioctahedral smectites involves open-system aqueous alteration of basaltic detritus in the lake, near the time of deposition, with elemental mobilization and oxidation driven by periodic desiccation and migration of the water table. Trioctahedral smectites may be the remnants of early-stage alteration of olivine or pyroxene, as proposed for YKB (*2-5*), or the product of high Mg^{2+} activities in lake water and sedimentary pore water caused by evaporation (*31*). Higher dehydroxylation temperatures indicate elevated Mg content in Murray saponite compared with YKB - a finding that is consistent with salinity-driven clay mineral formation mechanisms (*28*).

Although Oudam contains just ~3 wt.% phyllosilicates, their basal (*001*) diffraction at ~9.6 Å is distinct from those of every other phyllosilicate-bearing sample measured by CheMin to date. Interlayer collapse to <10 Å, potentially induced by the dry air inside CheMin (*4*), is observed in certain smectites with small, monovalent cations, such as Na^{+}, in the interlayer (*32*). However, we do not think the ~9.6 Å peak in Oudam stems from collapsed smectite. Other smectite-bearing samples maintain basal spacings of ~10 Å inside CheMin, indicating the prevalence of bivalent interlayer cations (*4*). No evidence of a process leading to the preferential Na-exchange of Oudam clays is apparent from rover observations. Instead, Oudam siltstones appear to have been bathed in Ca^{2+}-rich fluids as shown by Ca-sulfate minerals in the matrix (Table 1).

A basal diffraction of ~9.6 Å is also characteristic of high-charge or zero-layer-charge phyllosilicates that lack interlayer H_2O, which include certain micas (e.g., paragonite, margarite) and species in the pyrophyllite-talc series (e.g. ferripyrophyllite). The EGA trace for Oudam shows a single H_2O release at 470°C, which is reasonably attributable to dehydroxylation of a Fe(III)-rich phyllosilicate (*21*). Ferripyrophyllite is consistent with both XRD and EGA data (*33*).

All of the candidate 9.6 Å phyllosilicate analogs recognized are the products of high-temperature hydrothermal and metamorphic processes. The absence of textural or mineralogical indicators of these processes at Oudam, and the presence of sedimentary structures indicative of an aeolian origin (*14*), leads us hypothesize that Oudam phyllosilicates did not form *in situ*, but are wind-blown detritus sourced elsewhere (*29*).

Discussion

The contrast between the clay mineralogy of the Marimba, Quela, and Sebina mudstones with that of the 9.6 Å phyllosilicate in Oudam provides additional support linking smectite abundance and speciation with syn-depositional neoformation and transformation processes rather than later period of genesis during burial diagenesis. We note that the Oudam sample has the same basic mineralogy as other Murray formation mudstones (Table 1), much of which could serve as precursors to smectite formation in an invasive diagenetic fluid model (e.g., *26*). In terrestrial sedimentary basins, the high porosity and permeability typical of sandstones promotes more extensive production of burial diagenetic clay minerals compared with mudstones. Based on sedimentological observations it appears that Oudam sediments spent less time in a dynamic aqueous environment close to the water table.

The discovery of a broad spectrum of mineralogical facies at Gale crater provides a window into the history of near-surface aqueous alteration processes on ancient Mars. On Earth, aqueous reactions at the juncture of the atmosphere, hydrosphere and lithosphere (termed the critical zone) are central to biogeochemical cycles that regulate climate and biological productivity of the planet through the draw-down of greenhouse gases and release of nutrients (*34*). The unexpected abundance and diversity of clay minerals in sedimentary rocks at Gale crater and longevity of this sedimentary system (*2*) indicate near-surface aqueous alteration continued into the Early Hesperian on Mars. When integrated with sedimentological observations, clay mineral diversity provides additional insight into how environmental conditions evolved during and after the deposition of the strata of lower Aeolis Mons. Through the continued survey of sedimentary rocks at Gale, which are predicted to encompass a range of conditions, MSL has the opportunity to develop an understanding of how the martian critical zone operated and influenced planetary evolution.

Materials and Methods

CheMin collects X-ray diffraction (XRD) data using Co radiation in transmission geometry (see ref. *35* for more details). Curiosity's Sample Acquisition, Processing, and Handling (SA/SPaH) system was used to drill Oudam, Marimba, Quela, and Sebina from the Murray fm. bedrock (the majority of sample powder delivered to CheMin comes from a depth of 5 to 6 cm), sieve the resulting powder to <150 μm, and deliver ~50 mm^3 of material to CheMin analysis cells, which have either Mylar or Kapton windows. Oudam and Marimba were delivered to Mylar cells, and Quela and Sebina were delivered to Kapton cells. Sample cells are reusable and located on a rotating sample wheel. The cells are shaken piezoelectrically during analysis to randomize grain orientations, presenting all lattice orientations to the incident Co X-rays. A CCD detector is used to determine the energy and position of photons striking the CCD; fluoresced photons provide XRF data and the two-dimensional (2D) position of each diffracted Co Kα photon is used to construct the diffraction pattern; circumferential integration of Debye diffraction rings, corrected for arc length, produces a conventional 1D XRD pattern with 2θ resolution of ~0.3° (e.g. Fig. 3). Positions of detected photons are summed over repeated 10-sec measurements for several hours during each night of analysis. Samples are generally analyzed for four or more nights, spaced at time intervals determined by rover energy budget, allowance for operating other instruments, and other operational considerations. Plagioclase is a common phase in almost all samples, and the 1D diffraction patterns are corrected for minor variations in sample-to-detector distance using the best fit to plagioclase c and γ unit cell parameters (*10*). Abundances of crystalline phases in the Oudam, Marimba, Quela, and Sebina samples were determined by Rietveld analysis using Jade software. The mineral quantities presented in this paper (Table 1) differ slightly from results available in the Planetary Data System (PDS) (https://pds.nasa.gov). These new results are products of Jade-based Rietveld refinements that incorporate clay mineral standard patterns in addition to structural models of crystalline phases. We find this method improves model fits of measured XRD patterns.

The clay mineral standards used in these hybrid refinements were measured on CheMin 4 – a prototype instrument that is similar to the CheMin flight instrument. We found that including both dioctahedral and trioctahedral smectite clay mineral standards led to the best replication of measured XRD patterns in Jade, consistent with our conclusion that Marimba, Quela, and Sebina

contain both di- and trioctahedral smectite phases. Smectite clay mineral standards were heated to 200ºC for 10 hours before analysis to remove interlayer H_2O and collapse basal spacing to ~10 Å, to more closely replicate the state of clay minerals within MSL. These approaches produce accurate identification and detection for virtually all crystalline phases at abundances greater than ~1 wt.%. The abundances of amorphous components and poorly crystalline clay minerals are determined using the program FULLPAT (*36*) and remain as reported in the PDS.

The phases contributing to the pattern in the vicinity of the clay mineral 02*l* band were examined in more detail using BGMN, a Rietveld refinement program that can generate XRD patterns of partially disordered clay minerals and simultaneously consider contributions from crystalline phases (*37*,*38*). BGMN uses instrument profiles as part of the XRD pattern modeling procedure. BGMN instrument profiles are generated based on description of the XRD instruments' geometry using raytracing simulations. BGMNs' ray tracer does not support simulation of the flat CCD detector that collects CheMin patterns; therefore, we approximate profiles using a point detector, making adjustments to instrument geometry parameters until the profile function reproduces unit cell parameters and peak shapes of the beryl standard that resides inside CheMin and was measured earlier in the mission.

BGMN refinements were used to estimate the relative proportions of dioctahedral and trioctahedral smectites in Marimba, Quela and Sebina. These refinements include structural models of dehydrated dioctahedral smectite (based on montmorillonite) and a trioctahedral smectite (saponite). The b-unit cell parameter of the dioctahedral smectite phase was constrained to <9 angstroms during refinements, based on the relation between dehydroxylation temperature and Fe content of dioctahedral smectites in ref. *25*. Note that we report the ratios of dioctahedral:trioctahedral smectites from BGMN refinements because we do not have a reliable way to quantify the amount X-ray amorphous material in our samples with BGMN.

To distinguish between illitic and smectitic clay minerals, we use potassium abundance data obtained by the APXS onboard the Curiosity rover for Murray formation samples analyzed between sols 782 and 1496. These data are reproduced in Table S2 with their reported analytical uncertainties. A complete description of the instrument, as well as the methods used for calibration and quantification of APXS data, can be found in Gellert et al. (*39*) and Campbell et al. (*40*). In summary, APXS is a contact instrument with Curium-244 sources that induce Particle-Induced X-ray Emission (PIXE) and X-ray Fluorescence (XRF) to determine the

abundance of major, minor, and trace elements from sodium to bromine in soil and rock targets. Low atomic number (Z) element X-rays stem from the topmost 5 microns of the sample, higher Z elements like Fe are detected from the upper ~50 microns. The APXS is mounted on a turret at the end of the Curiosity rover's arm and is deployed on selected targets along the rover traverse to determine their elemental composition. The sampled area is about 1.7 cm in diameter when the instrument is in contact with the sample, and APXS spectra represent the average composition over the sampled area.

The Sample Analysis at Mars (SAM) instrument suite consists of a quadrupole mass spectrometer (QMS), a six-column gas chromatograph (GC), and a tunable laser spectrometer (TLS) connected to a gas processing system that includes two pyrolysis ovens (*24,41,42*). Gases evolved during pyrolysis of samples can be sent to several of these instruments; here we focus on data from the direct QMS detection of gases during sample heating, referred to as evolved gas analysis mass spectrometry (EGA-MS). Volatiles evolved during pyrolysis and their evolution temperatures can be used to inform the mineralogy or organic chemistry of samples. For further information about the SAM instrument and its operation see refs. *24,41,42*.

Splits of the <150 μm portion of the Oudam and Marimba sample powders were delivered by SA/SPaH into cleaned (by heating to >800°C) quartz sample cups. The mass of portions delivered to SAM cups is not measured *in situ* but is estimated to be 45 ± 18 mg (2σ) based on sample volume delivered during experiments with the Collection and Handling for Interior Martian Rock Analysis (CHIMRA) system testbed on Earth and analytical models (*41,42*). Sample fines were then heated from ~30°C (ambient SAM temperature) to ~860°C at 35°C /min under a helium carrier gas flow of ~0.8 standard cubic centimeters per minute (sccm) and ~25 mb of gas pressure in the sample pyrolysis ovens. A split of gases evolved from the sample during heating was swept into the QMS inlet and detected by the mass-to-charge ratio (m/z) of the molecules. If the main mass of a molecule saturated the MS detector, as was the case for m/z 18 from H_2O, then a signal for an isotopolog (e.g., $H_2{}^{18}O$ at m/z 20 for H_2O) or QMS fragment of the molecule (e.g., m/z 17 for H_2O) was used to study the evolution of a molecule with temperature.

Supplementary Materials

table S1. Data used to infer the K content of clay minerals.
fig. S1. Comparison of the clay mineral and potassium content of Murray formation samples.
fig. S2. Comparisons of CRISM smectite signatures in the Murray Formation vs. the phyllosilicate trough.

References and Notes

1. J. P. Grotzinger et al., A Habitable Fluvio-Lacustrine Environment at Yellowknife Bay, Gale Crater, Mars. *Science* **343**, 1242777 (2014).
2. J. P. Grotzinger et al., Deposition, exhumation, and paleoclimate of an ancient lake deposit, Gale crater, Mars. *Science* **350**, aac7575 (2015).
3. D. T. Vaniman et al., Mineralogy of a Mudstone at Yellowknife Bay, Gale Crater, Mars. *Science* **343**, 1243480 (2014).
4. T. F. Bristow et al., The origin and implications of clay minerals from Yellowknife Bay, Gale crater, Mars. *Am. Mineral.* **100**, 824-836 (2015).
5. S. M. McLennan et al., Elemental geochemistry of sedimentary rocks at Yellowknife Bay, Gale Crater, Mars. *Science* **343**, 1244734 (2014).
6. P. R. Mahaffy et al., The imprint of atmospheric evolution in the D/H of Hesperian clay minerals on Mars. *Science* **347**, 412–414 (2015).
7. E. B. Rampe et al., Mineralogical trends in mudstone deposits from the Murray formation, Gale crater, Mars. *Earth Planet. Sci. Lett*., **471**, 172-185 (2017).
8. J. A. Hurowitz et al., Redox stratification of an ancient lake in Gale Crater, Mars. *Science* **356**, eaah6849 DOI:10.1126/science.aah6849 (2017).
9. A. H. Treiman et al. Mineralogy, provenance, and diagenesis of a potassic basaltic sandstone on Mars: CheMin X-ray diffraction of the Windjana sample (Kimberley area, Gale Crater). *J. Geophys. Res. Planets* **121**,75–106 (2016).
10. S. M. Morrison et al., Crystal chemistry of martian minerals from Bradbury Landing through Naukluft Plateau, Gale crater, Mars. *Am. Mineral.* (In press).
11. C. E. Weaver, *Clays, Muds and Shales* (Developments in Sedimentology, Elsevier, New York, 1989), p. 819.
12. H. Chamley, *Clay Sedimentology* (Springer, Berlin, 1989), p. 623.
13. A. Meunier, *Clays* (Springer, Berlin, 2005), p. 472.
14. C. Fedo et al., Facies analysis and basin architecture of the upper part of the Murray Formation, Gale Crater, Mars. Lunar and Planetary Science Conference, The Woodlands, TX, Abstract **1689**, (2017).
15. S. Gwizd et al., Paleoenvironmental Assessment for the Hartmann'Vally Member, Murray formation, Gale crater, Mars. Lunar and Planetary Science Conference, The Woodlands, TX, Abstract **XXXX**, (2018).
16. N. Stein et al., Candidate desiccation cracks in the upper Murray formation, Gale crater, Mars. Lunar and Planetary Science Conference, The Woodlands, TX, Abstract **2387**, (2017).
17. B. Ehlmann et al., Subsurface water and clay mineral formation during the early history of Mars. *Nature* **114,** 53-60 (2011).
18. J. Carter, F. Poulet, J. P. Bibring, N. Mangold, S. Murchie, Hydrous minerals on Mars as seen by the CRISM and OMEGA imaging spectrometers: updated global view. *J. Geophys. Res., Planets* **118,** 831–858 (2013).

19. J. R. Michalski, J. Cuadros, J. L. Bishop, M. Darby Dyar, V. Dekov, and S. Fiore, Constraints on the crystal-chemistry of Fe/Mg-rich smectitic clays on Mars and links to global alteration trends, *Earth Planet. Sci. Lett.,* **427**, 215–225 (2015).
20. D. M. Moore and R. C. Reynolds, X-ray Diffraction and the Identification and Analysis of Clay Minerals (Oxford Univ Press, New York, 1997), *p. 382.*
21. L. Heller-Kallai, and I. Rozenson, Dehydroxylation of dioctahedral phyllosilicates. *Clays Clay Miner.* **28**, 355-368 (1980).
22. A. Derkowski, V. A. Drits and D. K. McCarty, Nature of rehydroxylation in dioctahedral 2:1layer clay minerals. *Am. Min*., **97**, 610–629 (2012).
23. J. Cuadros, J. Michalski, V. Dekov, J. L. Bishop, S. Fiore, M. Darby Dyar, Crystal-chemistry of interstratified Mg/Fe-clay minerals from seafloor hydrothermal sites. *Chem. Geol.* **360–361**, 142–158 (2013).
24. D. W. Ming et al., Volatile and Organic Compositions of Sedimentary Rocks in Yellowknife Bay, Gale Crater, Mars, *Science* **343**, (2014).
25. M. F. Brigatti M.F. Relationships between composition and structure in in Fe-rich smectites. *Clay Miner*. **18,** 177-186 (1983).
26. A. A. Fraeman et al., The stratigraphy and evolution of lower Mount Sharp from spectral, morphological, and thermophysical orbital data sets: stratigraphy and evolution of Mount Sharp. *J. Geophys. Res., Planets* (2016).
27. J. Carter, B. Gondet, Y. Langevin (2016), MSL Homing in on a large smectite clay deposit: An orbital perspective. Lunar and Planetary Science Conference, The Woodlands, TX, Abstract **1899**, (2016).
28. T. F. Bristow and R. E. Milliken, Terrestrial perspective on authigenic clay mineral production in ancient martian lakes. *Clays Clay Min.* **59**, 339-358 (2011).
29. J. Buz, B. L. Ehlmann, L. Pan, and J. P. Grotzinger, Mineralogy and stratigraphy of the Gale crater rim, wall, and floor units, *J. Geophys. Res. Planets,* **122**, 1090–1118 (2017) doi:10.1002/ 2016JE005163.
30. N. M. Mangold et al., Open-System Weathering at Gale Crater from the Chemistry of Mudstones Analyzed by the Curiosity Rover. Early mars Conference, Flagstaff, Abstract **3013** (2017).
31. V. C. Hover, L. M. Walter, D. R. Peacor, A. Martini, Mg-smectite authigenesis in a marine evaporative environment, salina Ometepec, Baja California. *Clays Clay Min.,* **47**, 252-268 (1999).
32. T. Sato, T. Watanabe, R. Otsuka, Effects of layer charge, charge location, and energy change on expansion properties of dioctahedral smectites. *Clays Clay Min.,* **40**, 103-113 (1992).
33. F. V. Chukhrov, B. B. Zvyagin, V. A. Drits, A. I. Gorshkov, L. P. Ermilova, E. A. Goilo, E. S. Rudnitskaya, The ferric analogue of pyrophyllite and related phases. Proceedings of the International Clay Conference, Oxford, 55-64 (1978).
34. R. Amundson, D. D. Richter, G. S. Humphreys, E. G Jobbágy, J. Gaillardet, Coupling between biota and Earth materials in the Critical Zone. *Elements* **3**, 327-332 (2007).
35. D. F. Blake et al., Characterization and calibration of the CheMin mineralogical instrument on Mars Science Laboratory. *Space Sci. Rev.* **170**, 341–399 (2012).
36. S. J. Chipera and D. L. Bish, FULLPAT: A full-pattern quantitative analysis program for X-ray powder diffraction using measured and calculated patterns. *J. Appl. Crystallogr.* **35**, 744–749 (2002).

37. J. Bergmann, P. Friedel, R. Kleeberg, BGMN a new fundamental parameter-based Rietveld program for laboratory X-ray sources, its use in quantitative analysis and structure investigations. *CPD Newsletter*, **20,** 5–8 (1998).
38. Ufer, K., G. Roth, R. Kleeberg, H. Stanjek, R. Dohrmann, J. Bergmann, Description of X-ray powder pattern of turbostratically disordered layer structures with a Rietveld compatible approach. Zeitschrift fur Kristallographie Supplements, **219,** 519–527 (2004).
39. R. Gellert et al., The Alpha Particle X-Ray Spectrometer (APXS): Results from Gusev Crater and calibration report. J. Geophys. Res. 111, E02S05 (2006).
40. J. L. Campbell et al., Calibration of the Mars Science Laboratory Alpha Particle X-ray Spectrometer. Space Sci. Rev. 170, 319–340 (2012).
41. P. R. Mahaffy, et al., The sample analysis at Mars investigation and instrument suite. *Space Sci. Rev*., **170**, 401-478 (2012).
42. L. A. Leshin, et al., Volatile, Isotope, and Organic Analysis of Martian Fines with the Mars Curiosity Rover, *Science* **341,** 6153 (2013).

Acknowledgements: We are grateful to R. Kleeberg who helped developed the CheMin instrument profile model for BGMN and A. Derkowski for informative discussion. S. Hillier and J. Michalski are thanked for constructive reviews. We acknowledge the support of the Jet Propulsion Lab engineering and management teams, and MSL science team members who participated in tactical and strategic operations, without whom the data presented here could not have been collected. Some of this research was carried out at the Jet Propulsion Laboratory, California Institute of Technology, under a contract with the National Aeronautics and Space Administration. SG acknowledges funding from the UK Space Agency (UKSA) (Grants: ST/J005169/1 and ST/N000579/1). A.C.M. and B.M thank NASA's MSL Participating Scientist program for supporting this effort. **Author contributions:** T.F.B. wrote the manuscript, with corrections, discussions, and/or revised text from coauthors. D.F.B., J.A.C., R.G., J.P.G., P.R.M., D.T.V. and A.R.V. were key in designing instruments and guiding the mission. All authors analyzed data and performed operational roles in data collection. **Competing interests:** The authors declare that they have no competing interests. **Data and materials availability:** All data discussed in this manuscript is available from the PDS (https://pds.nasa.gov/) and the Astrobiology Habitable Environments Database (http://odr.io/CheMin). Files and models required to replicate XRD refinements are available upon request.

Figures and Tables

Table 1. Mineralogical composition (wt. %) of Oudam, Marimba, Quela, and Sebina with 1σ errors. Detection limits for crystalline materials are 0.5 wt.%.

mineral	Oudam	Marimba	Quela	Sebina
Andesine	27.8 ± 0.5	14.0 ± 0.9	13.5 ± 0.7	10.7 ± 0.4
Hematite	13.9 ± 0.4	6.4 ± 0.4	7.1 ± 0.4	6.9 ± 0.2
Ca-sulfate	6.3 ± 0.3	7.0 ± 0.6	5.5 ± 0.4	7.4 ± 0.6
Sanidine	-	2.4 ± 0.6	2.3 ± 0.5	1.4 ± 0.4
Pyroxene	5.3 ± 0.9	0.7 ± 0.6	2.7 ± 0.7	2.8 ± 0.4
Jarosite	-	At detection	At detection	0.9 ± 0.2
Quartz	0.7 ± 0.1	At detection	At detection	At detection
Clay Minerals	3 ± 1	28 ± 5	16 ± 3	19 ± 4
Amorphous	43 ± 20	40 ± 20	51.7 ± 25	51.1 ± 25

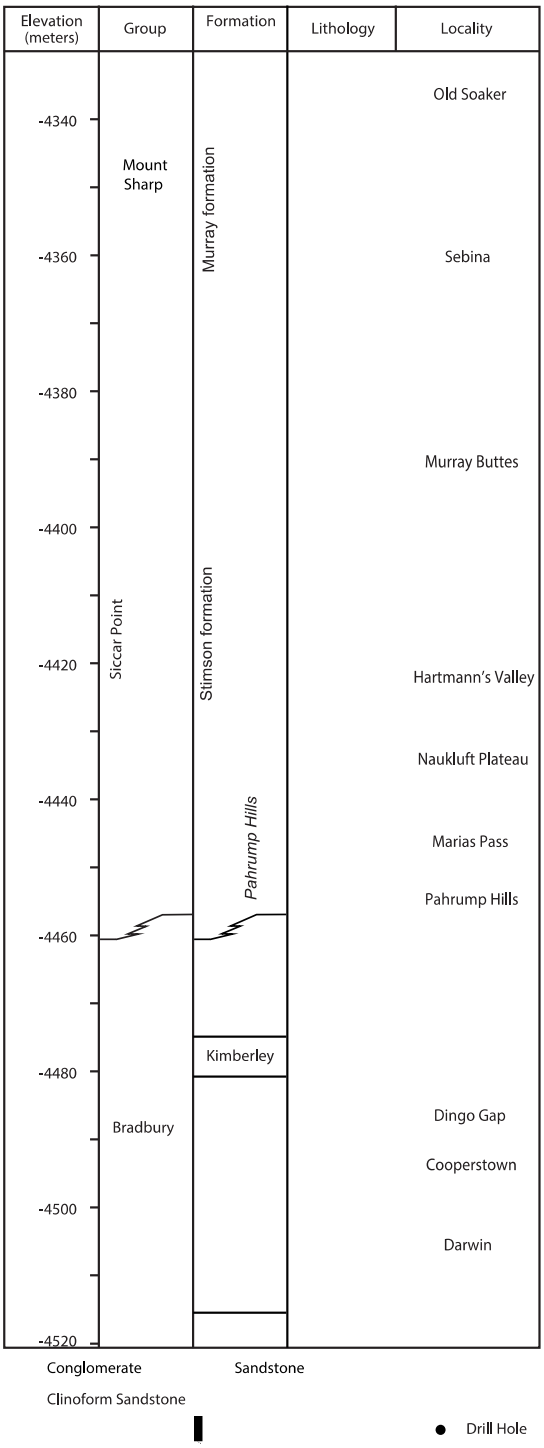

Figure 1. Stratigraphic column of sedimentary rocks at Gale crater observed by MSL, showing positions of drill samples. The stratigraphic framework of Gale crater sediments shown here was established in ref. 2 and is actively updated and refined through the efforts of the MSL sedimentology/stratigraphy working group (e.g. ref. *14*).

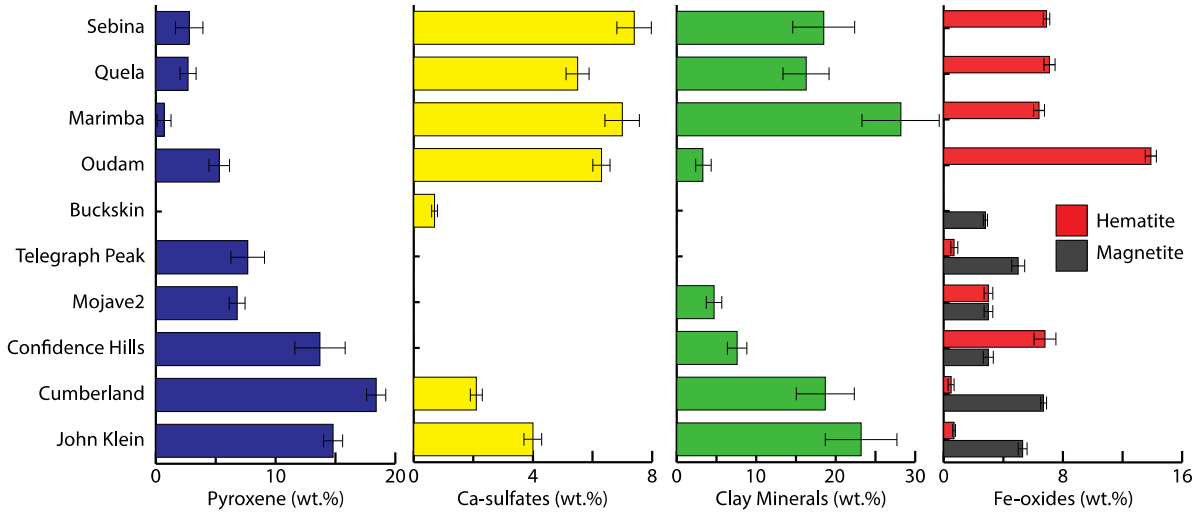

Figure 2 – Changes in abundances of environmentally sensitive mineralogical components in mudstones along MSLs' traverse. Samples are arranged in stratigraphic order. Mineral abundances and associated 1σ errors shown for John Klein and Cumberland, Confidence Hills to Buckskin, and Oudam to Sebina, are sourced from ref. 10, 7 and table 1, respectively.

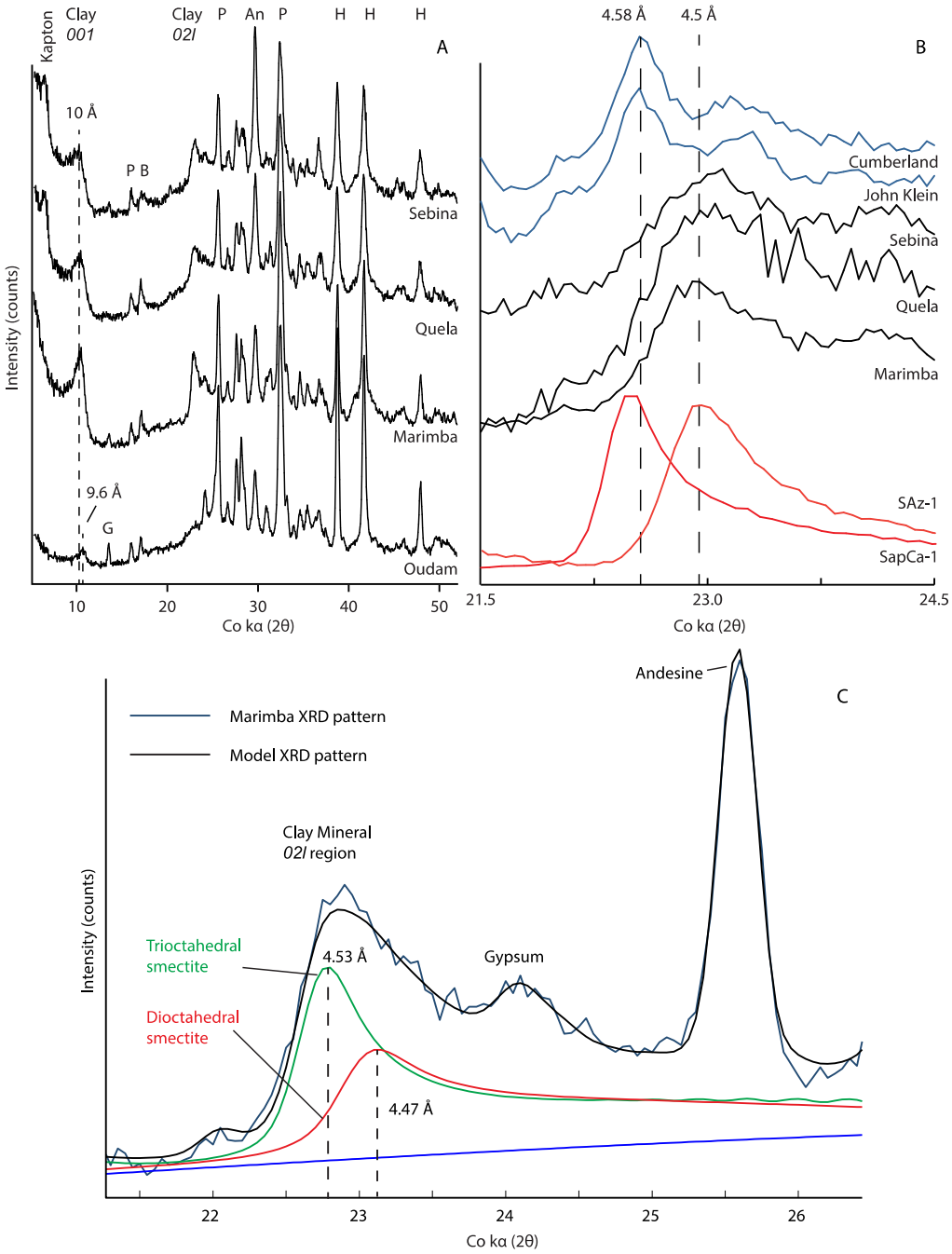

Figure 3. X-ray diffraction patterns of clay mineral bearing sample from Gale Crater. (A) Comparison of XRD patterns from Oudam, Marimba, Quela, and Sebina, with peaks assigned to clays minerals and other component minerals (A = anhydrite, B = bassanite, H = hematite, P = plagioclase). (B) Close up comparison of Marimba, Quela, Sebina, and YKB XRD patterns with trioctahedral and dioctahedral smectite standards (SapCa-1 saponite and SAz-1 montmorillonite), showing the difference in 02*l* band position corresponding to a difference in octahedral occupancy. (C) BGMN model of the 02*l* region of Marimba showing contributions from trioctahedral and dioctahedral smectites.

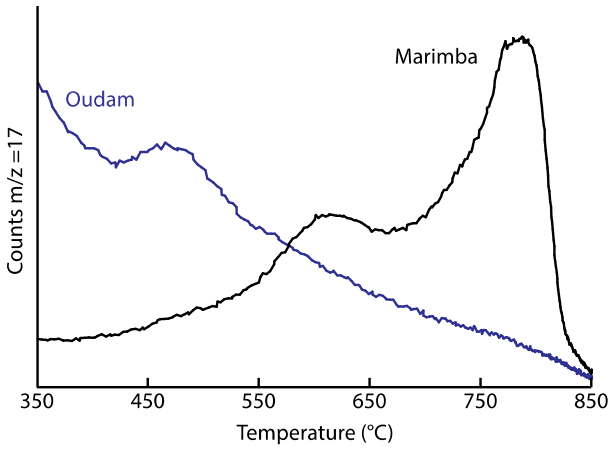

Figure 4 – SAM evolved H_2O release of Marimba and Oudam. Background has been subtracted from the EGA traces, the counts are not scaled.